Detectability of Fault Signatures in a Wastewater Treatment Process

Heidi L. Marais[1] Valentina Zaccaria[1] Jean-Paul A. Ivan[2] Eva Nordlander[1]

[1]Future Energy Center, Mälardalen University, Sweden, {heidi.marais, valentina.zaccaria, eva.nordlander}@mdh.se
[2]Center for Applied Autonomous Sensor Systems, Örebro University, Sweden jean-paul.ivan@oru.se

Abstract

In a wastewater treatment plant reliable fault detection is an integral component of process supervision and ensuring safe operation of the process. Detecting and isolating process faults requires that sensors in the process can be used to uniquely identify such faults. However, sensors in the wastewater treatment process operate in hostile environments and often require expensive equipment and maintenance. This work addresses this problem by identifying a minimal set of sensors which can detect and isolate these faults in the Benchmark Simulation Model No. 1. Residual-based fault signatures are used to determine this sensor set using a graph-based approach; these fault signatures can be used in future work developing fault detection methods. It is recommended that further work investigate what sizes of faults are critical to detect based on their potential effects on the process, as well as ways to select an optimal sensor set from multiple valid configurations.
Keywords: fault detection, wastewater treatment, detectability, isolation

1 Introduction

Fault detection (FD) is an important part of process supervision; monitoring the state of the process, identifying undesirable states, and initiating action to prevent negative consequences (Isermann, 2006, pg. 13). The safe and reliable operation of a process depends on the process supervision, this is no less the case in a wastewater treatment plant (WWTP) where poor performance can result in the release of untreated wastewater subsequently endangering human health and the environment (Ryder, 2017). The successful implementation of automatic control also hinges on the quality of process supervision. Control and automation in WWTPs has historically lagged behind other industrial processes, but is becoming increasingly important as effluent standards have become more strict and processes move from wastewater treatment to recovery (Olsson et al., 2005).

In a WWTP there are numerous types of faults that can occur, such as instrument faults and process faults. Specific process faults that have been the focus of FD research include: a decrease in the growth rate of autotrophic bacteria causing a decrease in nitrification (Choi and Lee, 2004; Lee et al., 2003, 2004b,a; Yoo and Lee, 2006), a decrease in the growth rate of heterotrophic bacteria (toxicity fault) (Aguado and Rosen, 2008; Borowa et al., 2007; Garcia-Alvarez et al., 2009; Yin et al., 2017; Yu, 2012), a combined decrease in growth rate and increase in death rate of heterotrophic bacteria (inhabitation fault) (Aguado and Rosen, 2008; Garcia-Alvarez et al., 2009; Yin et al., 2017), a decrease in ammonification rate (Yu, 2012), and a decrease in the settling velocity to simulate a bulking fault (Aguado and Rosen, 2008; Choi and Lee, 2004; Garcia-Alvarez et al., 2009; Yoo and Lee, 2006).

Each of these faults possess a fault signature based on how they affect the measurable states. These fault signatures are independent of any particular FD strategy (Ding, 2013, pg. 52), and knowledge of their detectability and isolability can be beneficial when quantifying the performance of different FD methods (Basseville, 2001).

Sensors and measurement devices are pivotal to FD as they provide information about the state of the process. However, the hostile environment in a WWTP commonly places sensors at risk of, for example, clogging and biofouling (Li et al., 2017). This can result in high maintenance costs due to required cleaning and calibration. Additionally, the sensors themselves are costly, can disturb the process, and in some cases are unavailable. Due to this, it is important to strategically select and place sensors in order to obtain as much information as possible while minimising the costs associated with monitoring.

There are numerous ways to approach the problem of sensor placement, such as considering observability and redundancy within the process (Villez et al., 2016, 2020), or considering fault detectability and isolability (Krysander and Frisk, 2008; Jung et al., 2020). In this work we consider the latter approach, focusing also on the determination of fault signatures for common process faults within a WWTP.

This type of analysis has been done extensively in other fields. For example, in gas turbines analysing fault signatures based on sensitivity (Chen et al., 2015), correlation (Stenfelt et al., 2019), and measurement uncertainty (Chen et al., 2015; Zaccaria et al., 2020) are all common procedures to determine a sensor set. However, a correlation based method is not easily applicable to a WWTP. WWTPs consist of process units in series, with

similar biochemical mechanisms occurring in each unit. This structure inherently leads to high correlation between measurements in successive units and renders futile the use of correlation analysis for sensor selection.

An alternative approach is to utilise the structural information of the process model. In this method variables and equations are represented as separate node sets in a bipartite graph and a graph theoretic approach is used to select a minimal sensor set (Krysander and Frisk, 2008). This approach yields 'best case' results for an ideal system. Using a distinguishability criterion that facilitates the specification of thresholds on the probability of false alarms and missed detections the method can be extended to a more realistic case, and when combined with model analysis a greedy stochastic search method can be used to determine an optimal sensor set to satisfy the requirements (Jung et al., 2020)

In this work a combined approach is used. Simulations are performed to observe the effects of faults on the various measurements, and responses that are below noise thresholds are discarded. The remaining fault-measurement combinations are represented as a bipartite graph, with non-zero residuals specifying the edges. Detectability and isolability conditions are defined in terms of neighbourhoods on the graph, and both a greedy approach and a Monte Carlo approach are implemented to obtain a minimal sensor set to satisfy the requirements.

2 Method

2.1 Simulation

The Benchmark Simulation Model No. 1 (BSM1) was used for simulating the WWTP. The benchmark plant consists of five biological reactors in series, where two are anoxic (total volume 2000 m^3) and three are aerated (total volume 3999 m^3), the reactors are modelled with the Activated Sludge Model No. 1 (ASM1). The reactors are followed by a secondary settler with a volume of 6000 m^3 which is modelled as a nonreactive ten layer settler with the Takács model (Gernaey et al., 2014, pg. 9–10). The model assumes a constant temperature of 15 °C. The BSM1 is used with the two standard control loops for NO_3-N and dissolved oxygen control, with set-points of 1 $g\,N\,m^{-3}$ and 2 $g\,O_2\,m^{-3}$ respectively (Gernaey et al., 2014, pg. 55–56). The layout of the process is shown in Figure 1 with the control loops, and the locations where for this study it was considered feasible to place sensors.

The MATLAB Simulink implementation of the steady-state form of the BSM1 was run with constant influent. The steady-state model utilises ideal sensors in the control loop but is otherwise similar to the normal BSM1. This simulation set-up was used to be able to easily detect the new steady-state that is reached after a fault has occurred.

The simulation model was modified to allow for the introduction of process faults. These faults were added as bias faults, where the size of the step was a percentage of the normal value of the parameter. Table 1 shows the list of faults, along with the normal values for the single parameters. The fault sizes used for simulation were 1 %, 5 %, 10 %, 20 %, 30 %, 40 %, 50 %, and 75 %. Considering each fault fault-size combination as a unique fault, a total of $n_f = 96$ faults were tested.

Table 1. Summary of faults that were introduced to the system. The fault symbol shows whether there was an increase or a decrease in the parameter. All growth rates are maximum specific growth rates as used in the ASM1.

Faulty Parameter(s)	*Normal Value*	*Symbol*	*Fault No.*
Ammonification rate	0.05[a]	$+k_a$	1
		$-k_a$	2
Heterotrophic growth rate	4 d^{-1}	$+\mu_H$	3
		$-\mu_H$	4
Heterotrophic death rate	0.3 d^{-1}	$+b_H$	5
		$-b_H$	6
Heterotrophic growth rate Heterotrophic death rate	4 d^{-1} 0.3 d^{-1}	I[b]	7
Autotrophic growth rate	0.5 d^{-1}	$+\mu_A$	8
		$-\mu_A$	9
Autotrophic death rate	0.05 d^{-1}	$+b_A$	10
		$-b_A$	11
Settling velocity	NA[c]	$-v_s$	12

[a] The ammonification rate constant has units of $m^3\,gCOD^{-1}\,d^{-1}$.
[b] The inhabitation fault is a combination of $-\mu_H$ and $+b_H$.
[c] The settling velocity is calculated from the double-exponential settling velocity function and therefore has no single normal value.

The simulation was loaded from a predetermined steady-state and run for 50 days before introduction of a fault. After the fault was introduced the simulation continued until the system reached a new steady-state. The post-fault steady-state values were used for the residual analysis.

2.2 Sensors and Measurement Noise

The starting set of sensors was taken as those variables that are commonly measured and have available commercial sensors. These included flow rates (Q), dissolved oxygen (S_O), alkalinity (S_{ALK}), total suspended solids (TSS), as well as nitrate/nitrite nitrogen (S_{NO}), and ammonium/ammonia nitrogen (S_{NH}) (Olsson et al., 2005; Rieger et al., 2003). All six variables were considered to be measurable at the eight locations indicated in Figure 1. These locations are used as subscripts to describe a specific sensor, e.g. $S_{O,5}$ indicates the dissolved oxygen measurement in the fifth reactor. Additional flow rates were measured in the wastage (Q_w) and internal recycle (Q_a). It was also assumed that the oxygen mass transfer coefficient (K_La), which represents the airflow into the final reactor, is known or measured. This resulted in a starting set of 51 measurements; 40 concentration sensors, 10 flow rate

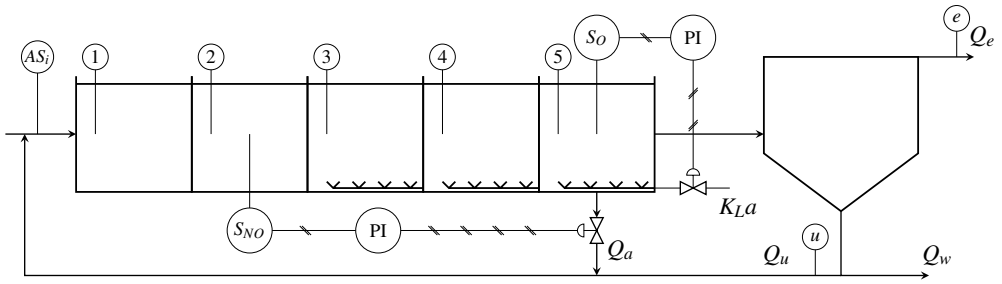

Figure 1. The plant layout for the BSM1 WWTP, the two standard control loops are shown on the diagram with the measurements involved, as well as all locations where it is assumed possible to install sensors and take measurements marked by 1-5 (inside biological reactors), e and u (in settler effluent and underflow respectively), and AS_i (in the inflow to biological reactors).

sensors, and the K_La value in the fifth tank. We represent the total number of sensors with n_s.

As stated previously, ideal sensors were used in the simulation of the process. However, sensor ranges and measurement uncertainty were considered when analysing the residuals. In the non-ideal BSM1 measurement noise is specified as 2.5 % of the maximum measurement range boundary for the sensor of interest, and measurement ranges for variable-specific sensors are provided (Gernaey et al., 2014; Rieger et al., 2003). We denote the measurement noise for sensor j as σ_j^2.

A sensitivity analysis was performed by changing the noise to 1 % (Rosen et al., 2008) and 4 % and comparing the main results.

2.3 Analysis of Residuals

Residuals were calculated for each fault, fault size, and sensor based on the normal operating conditions and the post-fault steady states obtained from simulations performed using the modified BSM1. These residuals form an $n_f \times n_s$ influence matrix M', where $M'_{i,j}$ represents the size of the residual detected by sensor j caused by fault i. We then construct an $n_f \times 2n_s$ binary influence matrix M as follows:

$$M_{i,j} = \begin{cases} 1, & M'_{ij} > \sigma_j^2 \\ 0, & \text{otherwise} \end{cases} \quad M_{i,j+n_s} = \begin{cases} 1, & M'_{ij} < -\sigma_j^2 \\ 0, & \text{otherwise} \end{cases} \tag{1}$$

If we represent this matrix blockwise $M = [M_+ M_-]$ then the block M_+ shows that fault i caused a positive residual above the noise threshold of sensor j; block M_- shows the same thing for negative residuals.

This can be interpreted as the biadjacency matrix of a bipartite graph $G = (F, S, E)$, where $F = \{f_i\}_{i=1}^{n_f}$ is a set of vertices representing faults, $S = \{s_j^+, s_j^-\}_{j=1}^{n_s}$ is a set of vertices representing positive or negative residuals on sensors, and E is the set of edges. A fault, f_i, is detectable only if it is connected to at least one sensor s_j^+ or s_j^-. Formally, we can say that the neighbourhood of a detectable fault in G is non-empty, i.e. $N(f_i) \neq \emptyset$. A fault can be isolated if it is detectable and the residual set it creates is distinct from all others, i.e. $N(f_i) = N(f_j)$ if and only if $i = j$.

Call a subgraph $H = (F, S', E')$ of G a minimal sensor graph if: 1) all faults which are detectable in G are detectable in H, 2) all faults which are isolable in G are isolable in H, 3) removing any vertex pair (s_j^+, s_j^-) from S' would violate 1) or 2). To find a minimal sensor graph in G we used both a greedy method for removing vertices from G, as well as a Monte Carlo approach.

For the greedy method residual pairs (s_j^+, s_j^-) are iterated through, if a pair is found which can be removed without affecting the overall isolability and detectability, it is removed. This continues until no more residual pairs can be removed. The Monte Carlo approach samples from the existing residual pairs randomly and removes pairs while preserving isolability and detectability. When the subgraph stagnates the search terminates.

3 Results and Discussion

Following the procedure detailed above, both the greedy method and the Monte Carlo approach identified a minimum of eleven sensors as necessary to detect and isolate the maximum number of fault cases. Ten thousand iterations of the Monte Carlo approach resulted in no changes to the minimum number of sensors, but different combinations of sensors were identified. Future work will investigate additional criteria which may be used to determine an optimal sensor set from the results of the Monte Carlo approach, however, this work considers the set obtained with the greedy method. These sensors are: $S_{NH,1}$, $S_{NH,3}$, $S_{NO,3}$, $S_{O,3}$, $S_{O,4}$, $S_{NO,e}$, $S_{ALK,e}$, TSS_e, TSS_u, $TSS_{AS_{in}}$, K_La_5.

3.1 Fault Detectability and Isolability

Considering the faults described in Table 1, faults $+k_a$ and $+\mu_H$ were found to be undetectable by any of the possible sensors, given the sensor noise thresholds. This is not unexpected as they were unconventional faults; increasing either of these parameters may in some circumstances be beneficial, however, any deviation from the desired operating point satisfies the definition of a fault.

Additionally, small deviations, the 1 % and 5 % fault sizes, were found to be undetectable. Considering that the smallest deviation in these parameters that was found in the literature was 6 % (Lee et al., 2003), with 40 % to 60 %

being more common sizes for changes in the parameters, this is an expected result. Future work should consider the effect that different fault sizes have on the performance of the WWTP in order to understand which sizes are critical to detect. These aforementioned non-detectable faults account for 36 of the original 96 tested faults.

Figure 2 shows for the detectable faults and fault sizes, at what size each fault became detectable, and where the signatures were unique. From this Figure we can see that 31 of the original 96 faults were detectable *and* isolable, while 43 were detectable.

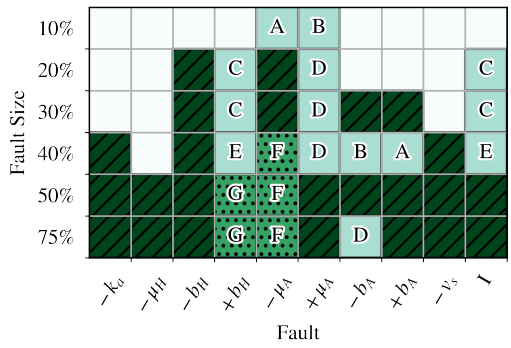

Figure 2. The detectability and isolability of faults is shown for different sizes of faults. White indicates an undetectable fault while colored indicates a detectable fault. The dark green with hatching shows completely unique fault signatures, green with a dotted pattern indicates that within a particular fault different sizes have the same signature, and the unpatterned light green shows identical signatures in different fault types. The letters show which fault signatures are the same.

There are several interesting observations to be made from this Figure. Firstly, we see that certain faults at particular sizes can resemble different faults at either the same, or different fault sizes. Consider the faults marked 'A' as an example of the latter case; this occurs at a 10 % deviation for fault $-\mu_A$, and at 40 % for $+b_A$ and shows that these two faults share the same signature. This makes sense as a decrease in growth rate and an increase in death rate of the autotrophic bacteria can be expected to have a similar effect on the process. However, the faults are distinguishable if their evolution is monitored as they only share a signature at one size. The faults marked 'B' and 'D' show a similar relationship between $+\mu_A$ and $-b_A$, but identical signatures also exist *within* the $+\mu_A$ fault across several sizes as shown by the 'D' faults.

Faults $+b_H$ and I are interesting due to the appearance of 'C' and 'E', marking two unique signatures shared by these two faults at the same sizes. This is likely due to the fact that I, as mentioned previously, is a combination of $+b_H$ and $-\mu_H$. In Figure 2, fault $-\mu_H$ is seen to be undetectable until a size of 50 %, this is the size at which the signatures of $+b_H$ and I become distinct from each other, indicating that at smaller sizes the dominant effect was $+b_H$ and we could expect the two signatures to be equal. From this observation we can state that it is likely that if an additional fault was tested that was the combination of $+b_A$ and $-\mu_A$, this fault would share signatures with $-\mu_A$ until fault size 30 %.

The uniqueness of signatures across fault sizes, within a fault, can be a useful property as fault sizes can be identified purely from the *signs* of the residuals, without analysis of the *size* of the residuals. In the case where certain fault sizes require immediate action this property can provide an early warning if the evolution of fault signatures are monitored.

3.2 Fault Signatures

Discussing now the fault signatures, in Figure 3 all fault signatures are shown. Each subplot is for a single fault, the columns represent the different sizes of the fault, and the rows show which sensor is used in detecting that occurrence of the fault. The sign of the residual is shown by the fill on the Figure.

The first observation to make from Figure 3 is that, when considering fault pairs of "+" and "−" of the same parameter, we observe similar residual patterns yet opposite signs. This is an expected response, and if the process were perfectly linear we would expect identical but oppositely signed residual patterns. There are three pairs to observe this behavior in: μ_A, b_A, and b_H.

Secondly, pairs of parameters that have a similar effect on the process have similar residual patterns. These pairs are the oppositely signed changes of growth and death rates of either the autotrophic or heterotrophic bacteria. This was mentioned in the discussion of Figure 2 in relation to the labelled pairs of identical signatures ('A', 'B', 'C', etc.). Considering 'C' and 'E' which were seen between faults $+b_H$ and I, these are easily identified in Figure 3. We see $S_{O,4}$, TSS_{AS_i}, TSS_u, and K_La_5 responding to both of these faults identically up until fault size 50 % where the effect of $-\mu_H$ becomes significant.

Considering some specifics, the sensor TSS_e is only used to detect a decrease in the settling velocity ($-v_s$). This suggests that despite this fault having a more complex signature based on the sensor set, it could be identified and isolated with that single sensor if the size of the fault was not of interest. Similarly, $S_{ALK,e}$ is only used in fault $-\mu_A$ and causes size 20 % and 30 % to be distinguishable. If we were uninterested in isolating the sizes of this fault based on the binary residual approach followed, this sensor could be excluded from the sensor set.

Finally, if we consider K_La_5 in the fault $-\mu_A$, the residual can be observed to change sign as the fault size increases which is a clear indicator of nonlinearities in the process.

3.3 Sensitivity to Measurement Noise

Sensitivity of the selected sensor set and detectable faults to measurement noise can be evaluated by repeating the analysis for different sensor noise levels. Table 2 shows the maximum possible number of isolable faults, the number of sensors required for fault isolation, and the changes

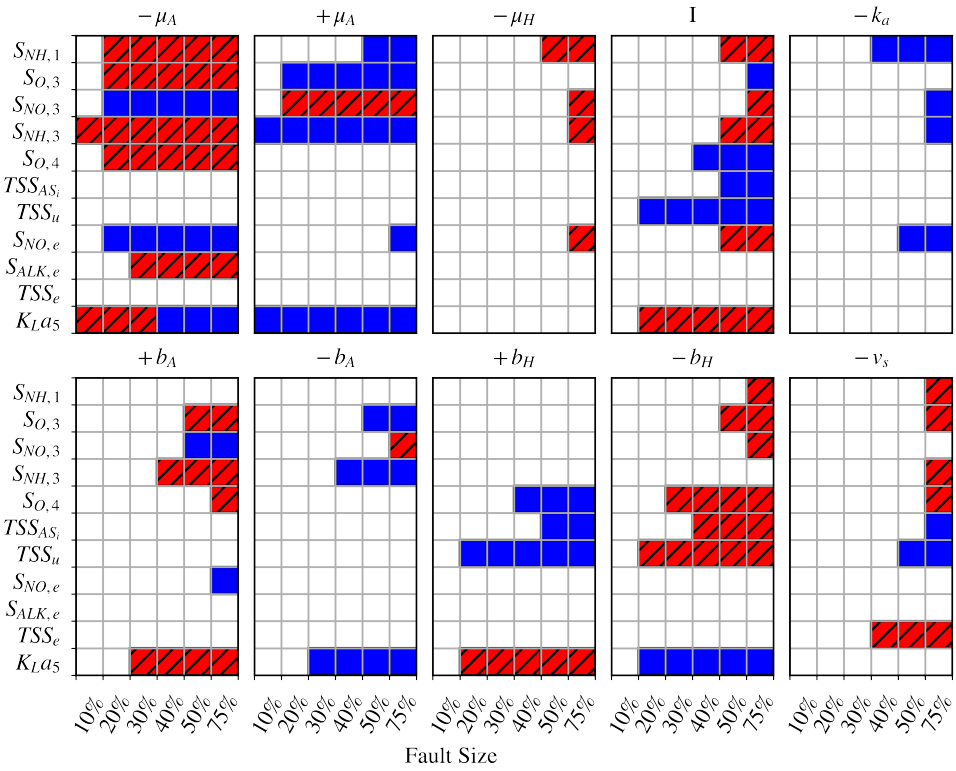

Figure 3. Fault signatures for the tested, detectable, faults. The hatched red squares indicate a positive residual observed in a specific sensor while unpatterned blue indicates a negative residual.

to the sensor configuration specified previously.

Table 2. Sensitivity of analysis to measurement noise.

	1 %	2.5 %	4 %
Isolable faults	34	31	31
Number of sensors	13	11	10
Sensors to remove	-	-	$S_{ALK,e}$, $S_{O,4}$
Sensors to add	$S_{NH,4}$, Q_a	-	$S_{NH,4}$

An interesting observation is the addition of sensor $S_{NH,4}$ in both cases, this suggests that including this sensor in the recommended sensor set may make the FD and isolation more robust to variations in noise and uncertainty. The additional number of sensors required to detect the faults with less noise is due to more sensors producing residuals above the threshold and subsequent isolation of the faults requiring more information. We can similarly discuss the fewer number of sensors required to isolate the same number of faults with the 4 % noise when compared to 2.5 %. As the noise increases the number of residuals above the threshold decreases, which means fewer sensors may be required to isolate the same number of faults. This suggests that clearly defining a threshold for each sensor is a vital step in the FD procedure.

4 Conclusions and Recommendations

Using a combined simulation based-graph theoretic approach a minimal sensor set was suggested in order to allow for the detection and isolation of the maximum number of fault fault-size combinations. The required sensors were $S_{NH,1}$, $S_{NH,3}$, $S_{NO,3}$, $S_{O,3}$, $S_{O,4}$, $S_{NO,e}$, $S_{ALK,e}$, TSS_e, TSS_u, $TSS_{AS_{in}}$, K_La_5; a total of eleven. However, other combinations of eleven sensors were capable of detecting the same faults and future work should consider how to select the optimal combination of sensors. It was found that replacing $S_{ALK,e}$ with $S_{NH,4}$ may increase the robustness to variations in measurement noise, and the importance of defining a noise threshold was highlighted.

Fault signatures were identified for faults relating to changes in the growth and death rates of the autotrophic and heterotrophic bacteria, as well as changes to the ammonification rate, and settling velocity. It was observed that small changes to these parameters do not produce residuals that are distinguishable from measurement noise, and it is recommended that future work investigate the effect that different fault sizes have on the performance of the WWTP in order to highlight which fault sizes are critical to detect.

The results were based on a binary approach, considering only the sign of the residual and not its magnitude. It may be possible to reduce the sensor set and increase isolability by considering residual magnitude, and this can be investigated further in future work. Following the binary approach simplifies the residual analysis and is easier to visualise; which is an important consideration in terms of potential implementation in industry.

5 Acknowledgements

This study has been done within the international project Control4Reuse with partners from Sweden, France and Brazil. The project is part of the IC4WATER programme, in the frame of the collaborative international consortium of the 2017 call of the Water Challenges for a Changing World Joint Programme Initiative (Water JPI). The authors would like to thank Formas (Project No 2018-02213) for funding the Swedish part of this project, within the above mentioned initiative.

References

D. Aguado and C. Rosen. Multivariate statistical monitoring of continuous wastewater treatment plants. *Engineering Applications of Artificial Intelligence*, 21(7):1080–1091, Oct. 2008. doi:10.1016/j.engappai.2007.08.004.

M. Basseville. On Fault Detectability and Isolability. *European Journal of Control*, 7(6):625–637, Jan. 2001. doi:10.3166/ejc.7.625-637.

A. Borowa, M. A. Brdyś, and K. Mazur. Detection of Unmeasured Process Abnormalities in Wastewater Treatment Process using MS-PCA. *IFAC Proceedings Volumes*, 40(9):262–267, Jan. 2007. doi:10.3182/20070723-3-PL-2917.00042.

M. Chen, L. Quan Hu, and H. Tang. An Approach for Optimal Measurements Selection on Gas Turbine Engine Fault Diagnosis. *Journal of Engineering for Gas Turbines and Power*, 137(7), July 2015. doi:10.1115/1.4029171.

S. W. Choi and I.-B. Lee. Nonlinear dynamic process monitoring based on dynamic kernel PCA. *Chemical Engineering Science*, 59(24):5897–5908, Dec. 2004. doi:10.1016/j.ces.2004.07.019.

S. X. Ding. *Model-Based Fault Diagnosis Techniques Design Schemes, Algorithms and Tools*. Advances in industrial control. Springer London, London, 2nd ed. edition, 2013. ISBN 978-1-4471-4799-2.

D. Garcia-Alvarez, M. J. Fuente, P. Vega, and G. Sainz. Fault Detection and Diagnosis using Multivariate Statistical Techniques in a Wastewater Treatment Plant. *IFAC Proceedings Volumes*, 42(11):952–957, Jan. 2009. doi:10.3182/20090712-4-TR-2008.00156.

K. V. Gernaey, U. Jeppsson, P. A. Vanrolleghem, and J. B. Copp. *Benchmarking of Control Strategies for Wastewater Treatment Plants*. IWA Publishing, Sept. 2014. ISBN 978-1-84339-146-3.

R. Isermann. *Fault-Diagnosis Systems: An Introduction from Fault Detection to Fault Tolerance*. Springer-Verlag, Berlin Heidelberg, 2006. ISBN 978-3-540-24112-6. doi:10.1007/3-540-30368-5.

D. Jung, Y. Dong, E. Frisk, M. Krysander, and G. Biswas. Sensor selection for fault diagnosis in uncertain systems. *International Journal of Control*, 93(3):629–639, Mar. 2020. doi:10.1080/00207179.2018.1484171.

M. Krysander and E. Frisk. Sensor Placement for Fault Diagnosis. *IEEE Transactions on Systems, Man, and Cybernetics - Part A: Systems and Humans*, 38(6):1398–1410, Nov. 2008. doi:10.1109/TSMCA.2008.2003968.

J.-M. Lee, C.-K. Yoo, and I.-B. Lee. Statistical Process Monitoring with Multivariate Exponentially Weighted Moving Average and Independent Component Analysis. *Journal of Chemical Engineering of Japan*, 36(5):563–577, 2003. doi:10.1252/jcej.36.563.

J.-M. Lee, C.-K. Yoo, S. W. Choi, P. A. Vanrolleghem, and I. Lee. Nonlinear process monitoring using kernel principal component analysis. *Chemical Engineering Science*, 59(1): 223–234, Jan. 2004a. doi:10.1016/j.ces.2003.09.012.

J.-M. Lee, C.-K. Yoo, and I.-B. Lee. Statistical process monitoring with independent component analysis. *Journal of Process Control*, 14(5):467–485, Aug. 2004b. doi:10.1016/j.jprocont.2003.09.004.

T. Li, M. Winnel, H. Lin, J. Panther, C. Liu, R. O'Halloran, K. Wang, T. An, P. K. Wong, S. Zhang, and H. Zhao. A reliable sewage quality abnormal event monitoring system. *Water Research*, 121:248–257, Sept. 2017. doi:10.1016/j.watres.2017.05.040.

G. Olsson, M. Nielsen, Z. Yuan, A. Lynggaard-Jensen, and J.-P. Steyer. *Instrumentation, Control and Automation in Wastewater Systems*. IWA Publishing, Apr. 2005. ISBN 978-1-900222-83-9.

L. Rieger, J. Alex, S. Winkler, M. Boehler, M. Thomann, and H. Siegrist. Progress in sensor technology - progress in process control? Part I: Sensor property investigation and classification. *Water Science and Technology*, 47(2):103–112, Jan. 2003. doi:10.2166/wst.2003.0096.

C. Rosen, L. Rieger, U. Jeppsson, and P. A. Vanrolleghem. Adding realism to simulated sensors and actuators. *Water Science and Technology*, 57(3):337–344, Feb. 2008. doi:10.2166/wst.2008.130.

G. Ryder. The United Nations world water development report, 2017: Wastewater: the untapped resource. Technical report, UNESCO World Water Assessment Programme, Paris, 2017.

M. Stenfelt, V. Zaccaria, and K. Kyprianidis. Automatic Gas Turbine Matching Scheme Adaptation for Robust GPA Diagnostics. In *Proceedings of the ASME Turbo Expo*, volume 6, Phoenix, United States, June 2019.

K. Villez, P. A. Vanrolleghem, and L. Corominas. Optimal flow sensor placement on wastewater treatment plants. *Water Research*, 101:75–83, Sept. 2016. doi:10.1016/j.watres.2016.05.068.

K. Villez, P. A. Vanrolleghem, and L. Corominas. A general-purpose method for Pareto optimal placement of flow rate and concentration sensors in networked systems – With application to wastewater treatment plants. *Computers & Chemical Engineering*, 139:106880, Aug. 2020. doi:10.1016/j.compchemeng.2020.106880.

S. Yin, X. Xie, and W. Sun. A Nonlinear Process Monitoring Approach With Locally Weighted Learning of Available Data. *IEEE Transactions on Industrial Electronics*, 64 (2):1507–1516, Feb. 2017. doi:10.1109/TIE.2016.2612161. Conference Name: IEEE Transactions on Industrial Electronics.

C. K. Yoo and I. Lee. Nonlinear multivariate filtering and bioprocess monitoring for supervising nonlinear biological processes. *Process Biochemistry*, 41(8):1854–1863, Aug. 2006. doi:10.1016/j.procbio.2006.03.038.

J. Yu. A nonlinear kernel Gaussian mixture model based inferential monitoring approach for fault detection and diagnosis of chemical processes. *Chemical Engineering Science*, 68(1): 506–519, Jan. 2012. doi:10.1016/j.ces.2011.10.011.

V. Zaccaria, A. D. Fentaye, M. Stenfelt, and K. G. Kyprianidis. Probabilistic Model for Aero-Engines Fleet Condition Monitoring. *Aerospace*, 7(6):66, June 2020. doi:10.3390/aerospace7060066.